AJNR

The Role of MR Angiography in the Pretreatment Assessment of Intracranial Aneurysms: A Comparative Study

William M. Adams, Roger D. Laitt and Alan Jackson

The Role of MR Angiography in the Pretreatment Assessment of Intracranial Aneurysms: A Comparative Study

William M. Adams, Roger D. Laitt, and Alan Jackson

BACKGROUND AND PURPOSE: With developments in coil technology, intracranial aneurysms are being treated increasingly by the endovascular route. Endovascular treatment of aneurysms requires an accurate depiction of the aneurysm neck and its relation to parent and branch vessels preoperatively. Our goal was to estimate the clinical efficacy of MR angiography (MRA) in the pretreatment assessment of ruptured and unruptured intracranial aneurysms. We compared MRA source data (axial acquired partitions), multiplanar reconstruction (MPR) of these data, as well as maximum intensity projection (MIP) and 3D-isosurface images with intraarterial digital subtraction angiography (IA-DSA).

METHODS: The study was performed in 29 patients with 42 intracerebral aneurysms. The MRA data were examined in four different forms—as axial source data, MPR images of the source data, and MIP and 3D isosurface–rendered images. A composite standard of reference for each aneurysm was then constructed using this information together with the IA-DSA findings by looking at aneurysm detection rate, aneurysm morphology, neck interpretation, and branch vessel relationship to the aneurysm. All techniques, including conventional IA-DSA, were then scored independently on a five-point scale from 1 (non diagnostic) to 5 (excellent correlation with the standard of reference) for each of the aneurysm components as compared with the composite picture. An overall score for each technique was also obtained.

RESULTS: Of the 42 aneurysms examined, 34 were small (<10 mm), six were large (10–25 mm), and two were giant (>25 mm). Three aneurysms were not detected with MRA. These were smaller than 3 mm and either in an anatomically difficult location (middle cerebral artery bifurcation) or obscured by adjacent hematoma. Two large aneurysms were depicted as undersized by IA-DSA owing to the presence of intramural thrombus shown by MRA axial source data. IA-DSA received the highest scores overall and in three of the four subgroups. Three-dimensional isosurface reconstructions scored higher than did IA-DSA for depiction of the aneurysm neck, although this difference was not significant. The MPR and 3D-isosurface images were comparable to those of IA-DSA in all categories. MPR images were particularly useful for defining branch vessels and the aneurysm neck. MIP images scored poorly in all subgroups ($P < .005$) compared with IA-DSA findings, except for in aneurysm detection. Source data images were significantly inferior to those of IA-DSA in all categories ($P < .005$).

CONCLUSION: MRA is currently inferior to IA-DSA in pretreatment assessment of intracranial aneurysms, and can miss small lesions (<3 mm). It can, however, provide complementary information to IA-DSA, particularly in anatomically complex areas or in the presence of intramural thrombus. If MRA is used in aneurysm assessment, a meticulous technique with reference to both axial source data and MPR is mandatory. The axial source data should not be interpreted in isolation. Three-dimensional isosurface images are comparable to those of IA-DSA and are more reliable than are MIP images, which should be interpreted with caution.

The role of endovascular treatment in the management of patients with intracranial aneurysms is increasing. This is largely due to developments in microcatheter technology and occlusive materials, in particular the Guglielmi detachable coil (GDC) (1, 2). Whether or not an aneurysm is suitable for endovascular occlusion with coils depends on a number of factors. These include the absolute size

of the aneurysm neck (3) and the neck size relative to aneurysm size and shape. Understanding the relationship of the aneurysm to both parent and branch vessels is also important for minimizing the risks of thromboembolic complications (4).

Intraarterial digital subtraction angiography (IA-DSA) is considered the standard-of-reference investigative tool for intracranial aneurysmal disease, but it is invasive and carries a 1% complication risk with a 0.5% rate of persistent neurologic deficit (5). In addition, detailed aneurysm assessment prior to endovascular treatment often requires multiple angiographic projections. With the development of MR angiography (MRA), the absolute reliance on IA-DSA for aneurysm detection and surgical planning is changing (6). Increasing matrix size and improved background tissue suppression mean that spatial resolution is approaching that of formal angiography and aneurysms with diameters smaller than 2 mm and vessels smaller than 1 mm can now be accurately detected (7). Three-dimensional time-of-flight (3D-TOF) MRA is now readily accepted as a noninvasive screening tool for familial aneurysmal disease (8) and has been used as an alternative to IA-DSA for the surgical management of aneurysmal subarachnoid hemorrhage (9).

Image analysis and presentation of MRA axial source data are important aspects of the visualization process. Despite acknowledged limitations, much reliance has been placed on maximum intensity projection (MIP) MRA (10, 11). Alternative postprocessing algorithms such as 3D-isosurface MRA may have benefits over this technique (12). Reference to axial source data should also be included in aneurysm assessment because of the potential for data misrepresentation introduced by reconstruction techniques (13).

This study was designed to define the value of 3D-TOF MRA for the pretreatment assessment of both ruptured and unruptured cerebral aneurysms. The study was performed in 29 patients with 42 intracerebral aneurysms. We assessed MRA in the form of axial source data, multiplanar reconstruction (MPR) of these axial data, and two different postprocessing techniques: MIP and 3D isosurface rendering. The MRA and IA-DSA images were combined to form a composite reference standard, against which each technique was assessed.

Methods

Patients

Thirty-six patients were initially recruited into the study. Those patients who required emergency clipping or coiling of an aneurysm (n = 7) prior to MR imaging were subsequently excluded. The resulting study group consisted 29 patients (24 female, five male; average age, 47 years), with 42 intracranial aneurysms, which were studied with both IA-DSA and 3D-TOF MRA (Table 1). These patients presented either with aneurysmal subarachnoid hemorrhage (SAH) (n = 20) or symptoms related to focal mass effect. In one patient with a positive family history, IA-DSA followed by MRA was performed for screening. Incidental aneurysms (n = 9) were also included in

TABLE 1: Patient presentation and aneurysm characteristics

Patient Age (yrs)/ Sex	Presentation	Location of Aneurysm	Size	Treatment
30/F	SAH 2° to AVM	LT Ophth.	4 mm	E
45/F	SAH	LT SCA	2 mm	Cons.
29/F	SAH	RT MCA*	2 mm	Cons.
		BT	2 mm	Cons.
34/M	SAH	BT	5 mm	NS exploration
49/F	Incidental	LT MCA	3 mm	Cons.
55/F	Mass effect	RT ICA	25 mm	EBO
45/F	SAH	ACoA	3 mm	E
44/F	SAH	LT MCA	2 mm	NS
		LT MCA	3 mm	NS
50/M	SAH	ACoA	7 mm	NS
74/F	SAH	ACoA	6 mm	E
61/F	Mass effect	LT ICA	14 mm	EBO
48/F	SAH	ACoA	7 mm	NS/E
55/F	Mass effect	LT ICA	18 mm	Declined
58/F	Mass effect	LT PComm	6 mm	NS
28/M	SAH	ACoA*	16 mm	NS
		LT ICA	2 mm	Cons.
40/F	Screening	LT ICA	4 mm	E
		RT MCA	5 mm	E
		RT Ophth	2 mm	Cons.
53/F	SAH	LT PComm	6 mm	NS
		RT PComm	5 mm	NS
51/F	SAH	ACoA	6 mm	NS
30/F	Mass effect	LT ICA	28 mm	Cons.
44/F	Mass effect	LT ICA	15 mm	E
43/F	SAH	RT PComm*	8 mm	NS
		RT MCA	4 mm	NS
47/F	SAH delayed	RT ICA	3 mm	Cons.
55/F	SAH	ACoA	12 mm	E
49/F	SAH	BT	9 mm	E
62/F	SAH	ACoA	7 mm	NS
48/F	SAH	LT ICA	6 mm	E
		ACoA	5 mm	E
		LT MCA	5 mm	Cons.
		LT MCA	3 mm	Cons.
		RT MCA	5 mm	Cons.
29/M	SAH	ACoA	3 mm	NS
41/M	SAH	RT PCA	8 mm	E
		RT Ophth.	5 mm	Cons.
		LT MCA	2 mm	Cons.
63/F	Mass effect	LT PComm	15 mm	NS

* Indicates the source of hemorrhage where multiple aneurysms were present and a source could be confidently identified.

E = endovascular; Cons. = conservative; NS = neurosurgical; EBO = endovascular balloon occlusion; opth. = ophthalmic; MCA = middle cerebral artery; SCA = superior cerebellar artery; BT = basilar termination; ICA = internal carotid artery; ACoA = anterior communicating artery; PComm = posterior communicating artery; i.m. = intramural.

the study and assessed separately. These included two patients who had MRA performed for follow-up of previously treated aneurysms. The diagnosis of SAH was made by either CT or lumbar puncture. In all cases of SAH, formal angiography was performed prior to MRA to identify the source of hemorrhage. In 35 of the 42 aneurysms, MRA was performed within 24 hours of IA-DSA. This allowed direct comparison between imaging techniques, minimizing possible errors introduced by the changing dynamics of the cerebral circulation following SAH.

In the remaining seven aneurysms, MRA was performed within 1 week of IA-DSA. The suitability of a patient with aneurysmal SAH for MR examination was decided on the basis of clinical grade and the patient's condition at presentation.

Image Acquisition

All IA-DSA studies were performed on an Integris V3000 fluoroscopy unit (Philips, Best, The Netherlands) with a 1024 × 1024 matrix. Selective three- or four-vessel angiography using a standard projection format (anteroposterior, lateral, periorbital, and reverse-oblique) was performed initially and then additional views were obtained, if required, to identify the parent vessel and aneurysm neck more clearly.

MR examinations were performed on a 1.5-T Gyroscan ACS NT unit (Philips) by use of a quadrature head coil. After a localizer scan was performed (100/20/1 [TR/TE/excitations]), a single-slice 2D phase-contrast sagittal angiogram (14/7 [TR/ TE]; field of view (FOV), 13 cm; matrix, 256 × 256; flip angle, 20°; peak velocity encoding rate, 30 cm/s) was performed to identify the circle of Willis. A 3D-TOF single-slab MRA acquisition (45/ 7; flip angle, 20°; FOV, 21 cm; matrix, 512 × 512; slice thickness, 0.7 mm with 100 contiguous slices) was then performed through the circle of Willis, giving an effective voxel size of 0.41 × 0.41 × 0.7 mm. Background tissue suppression was maximized by the addition of an off-resonance magnetization transfer gradient. Because no posterior inferior cerebellar artery (PICA) aneurysms were included in the study, the imaging volume did not routinely include the origin of PICA in order to reduce imaging time. An axial gradient spin-echo sequence (4689/110/4; FOV 23, cm; matrix, 256 × 179; echo train length, 7) through the brain was routinely performed in each case. The MR data were transferred to a Philips Easy Vision Release 2.12 workstation for viewing and postprocessing.

Viewing and Postprocessing

In order to ensure reproducibility, visualizations of MR data were produced by an experienced neuroradiologist (A.J.), who has considerable experience with image postprocessing. The hard-copy formal angiogram was reviewed first. MRA source images were displayed on the workstation in cine loop, and MPRs were generated and viewed interactively. Aneurysm size was assessed using MPR measurements along the maximum plane. MIP generation was performed to produce angiogram-like images. MIP generation was initially performed using whole data sets and subsequently repeated using closely targeted image volumes reduced to depict only the aneurysm and immediate relations. Three standard series of MIP reconstructions were produced, each consisting of 42 projections evenly spaced around a single rotational axis (foot-to-head, right-to-left, and front-to-back). Generation of whole-volume MIP images was completed in about 5 to 10 minutes, and generation of the MIP from a targeted volume took slightly less time. Each aneurysm was therefore rendered in multiple projections, including a comparable projection to the ''best'' DSA projection.

Surface extraction and 3D rendering also took about 10 minutes to perform. To obtain consistent results, threshold levels were determined using original axial images for reference to ensure against under- or overrepresentation of vessel lumen. If there was significant hematoma surrounding an aneurysm, an attempt was made to reduce the threshold level to exclude the hematoma from the postprocessed image.

Comparison of Visualization Techniques

Comparison of the visualization methods was complicated by the lack of a true standard of reference. Previous investigators (14) have approached this problem by use of a composite reference standard derived from multiple imaging tech-

TABLE 2: Wilcoxon matched-pairs signed-ranks test (IA-DSA vs. other techniques)

	Source Data	MPR	MIP	3D
Detection	$P < .005$	NS	NS	NS
Morphology	$P < .005$	NS	$P < .005$	NS
Neck	$P < .005$	NS	$P < .005$	NS
Vessels	$P < .005$	NS	$P < .005$	NS

Note.—MPR = multiplanar reformat; MIP = maximum intensity projection; 3D = three-dimensional isosurface reconstruction; NS = not significant. $P < .005$ indicates IA-DSA is superior to technique.

niques. In order to derive such a reference standard for the current study, all images were retrospectively reviewed nonblinded by two neuroradiologists (W.M.A., R.D.L.). DSA findings and all available MR data (the source images, MPR, and MIP and 3D isosurface–generated images) were viewed, and a consensus opinion was obtained regarding morphologic as well as neck and branch vessel characteristics of the aneurysm. Using all the available data, a composite picture of each aneurysm was constructed. This composite reference standard was used to describe the shape of the aneurysm, the size and shape of the neck, and the relationship of the aneurysm to parent and branch vessels. At the same time, measurements of aneurysm size were made from the MPR data.

In order to assess the performance of each imaging technique, results were reviewed, then scored on a five-point scale of confidence—1) nondiagnostic image quality; 2) poor agreement; 3) acceptable agreement; 4) good agreement; and 5) excellent agreement—against the above-described composite reference standard. Each technique was scored for aneurysm detection, aneurysm morphology, confidence at interpreting the neck, and confidence at interpreting the origin of branch vessels as arising from aneurysm or neck. This scoring was performed by consensus review by the two neuroradiologists who had initially derived the consensus standard-of-reference descriptions. The review was performed at a separate sitting 1 week after the images had been originally seen.

Assessment of the performance of each technique was performed by comparing overall average scores for each technique and by use of the Wilcoxon signed rank test (Table 2) to allow direct comparison between techniques (15).

Results

Of the 42 aneurysms studied, 34 were defined as small (<10 mm), six were large (10–25 mm), and two were giant (> 25 mm). Thirteen aneurysms were equal to or less than 3 mm in size. Eighteen aneurysms were in the distribution of the internal carotid artery, 10 were anterior communicating artery aneurysms, 10 were located in the middle cerebral artery, and four were in the posterior circulation (Table 1).

Ten patients (13 aneurysms) subsequently underwent endovascular treatment and 11 patients (15 aneurysms) craniotomy for surgical clipping or exploration. In one patient with an anterior communicating artery aneurysm, surgical clipping was not possible, and the aneurysm was wrapped and treated subsequently by endovascular means. Fourteen aneurysms were not treated.

Image quality of TOF-MRA was excellent in 27 cases and showed minimal blurring from movement artifact in two patients (two aneurysms). In

four cases, the aneurysm responsible for hemorrhage was surrounded by high-signal hematoma. Although the aneurysm in these cases could still be defined on axial source data and MPR images, there was significant degradation of MIP reconstructions.

The majority of aneurysms were displayed well by all techniques, including those shown by IA-DSA. Those aneurysms that were not detected even retrospectively by the source-data axial images (n = 3) were smaller than 3 mm, were in difficult locations such as the middle cerebral trifurcation, or could not be interpreted because of the presence of surrounding high T1 signal methemoglobin in those patients with parenchymal hematoma. Review of the axial source data and MPR images was useful in two aneurysms larger than 1 cm because of the presence of intramural hypointense thrombus, not depicted on the postprocessed or on the IA-DSA images. Edge-of-field saturation effects tended not to detract from aneurysm visualization because of the central location of most of the aneurysms around the circle of Willis or related to the major branches.

Interpretation of the axial source data and MPR images was technically more challenging than was interpretation of the reconstructed image. MPR was defined as any plane other than the true axial plane represented by the source data. If the axial plane was the appropriate plane in which to view a particular aneurysm, then the axial source data tended to score higher than did the MPR. The ability to orient the plane along curved structures was useful in aneurysms involving the basilar termination. In one basilar-tip aneurysm associated with a dysplastic terminal basilar artery having a short focal stenosis proximal to the aneurysm, MPR more accurately delineated the stenosis than did the isosurface-rendered image.

MPR and 3D-isosurface images were comparable to IA-DSA images in all categories (Table 2). Only in the category of aneurysm detection was MIP-MRA comparable to IA-DSA. In the categories of aneurysm morphology and confidence at interpreting neck and branch vessels, MIP-MRA performed poorly with respect to IA-DSA ($P < .05$). The axial source data images were significantly inferior to IA-DSA images in all categories ($P < .05$).

In the overall average scores for each technique (Fig 1), MPR underscored with respect to IA-DSA and 3D-isosurface images in showing aneurysm morphology, but was superior to MIP. IA-DSA was superior in each category, apart from depiction of the aneurysm neck in which 3D-MRA scored slightly higher. MPR was superior to MIP in every category except in aneurysm detection. When oriented in a particular plane, it was particularly useful for defining branch vessels and the neck of an aneurysm. MPR was superior to every other technique in the depiction of one middle cerebral artery bifurcation aneurysm. This was interpreted as a boot-shaped aneurysm with two limbs, one directed
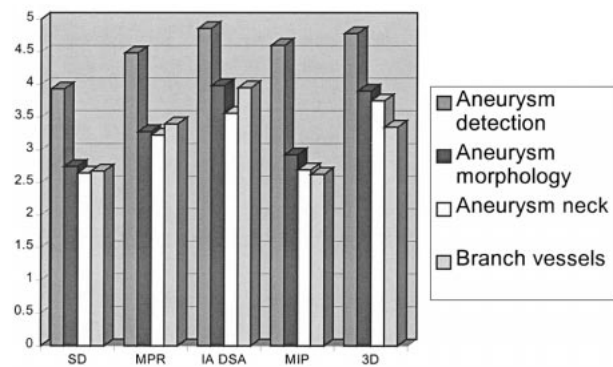

FIG 1.   Overall average score for each imaging technique. Note.— SD = source data; MPR = multiplanar reformat; IA DSA = intra-arterial digital subtraction angiography; MIP = maximum intensity projection; 3D = three-dimensional isosurface reconstruction.

inferiorly and one directed superiorly on IA-DSA, MIP, and 3D-isosurface images. MPR, however, suggested that there were in fact two separate aneurysms. This configuration was confirmed at surgery.

The MIP-MRA scored poorly for depiction of aneurysm morphology as well as for neck and branch vessel definition. Small vessels were poorly defined compared with other techniques (Fig 2). Depiction of aneurysm morphology was particularly poor compared with 3D-isosurface images. Turbulence or slow flow in complex aneurysms produced signal drop out. The lack of depth leading to poor spatial perspective on the reconstructed images was an additional factor responsible for its low scores.

In the majority of cases, MRA images were complementary to those of IA-DSA. Rather than adding clinical information, they confirmed the impression of an aneurysm gained from a DSA study. There were, however, four cases in which significant discrepancies occurred between techniques. These are individually described in the following cases.

Case 1

GDC embolization was attempted in a 55-year-old woman with SAH caused by a complex anterior communicating artery aneurysm. The 3D-isosurface MRA, although partly obscured by patient movement, had suggested that the A2 segments of the anterior cerebral artery on both sides originated from the aneurysm. Despite selective injections into the feeding A1 branch during arteriography, the origin of the A2 segments was still not clear. Cautious intraaneurysmal injections revealed the A2 origins and confirmed the MRA appearances. Coils were introduced but resulted in occlusion of both A2 branches and were therefore not deployed.

Case 2

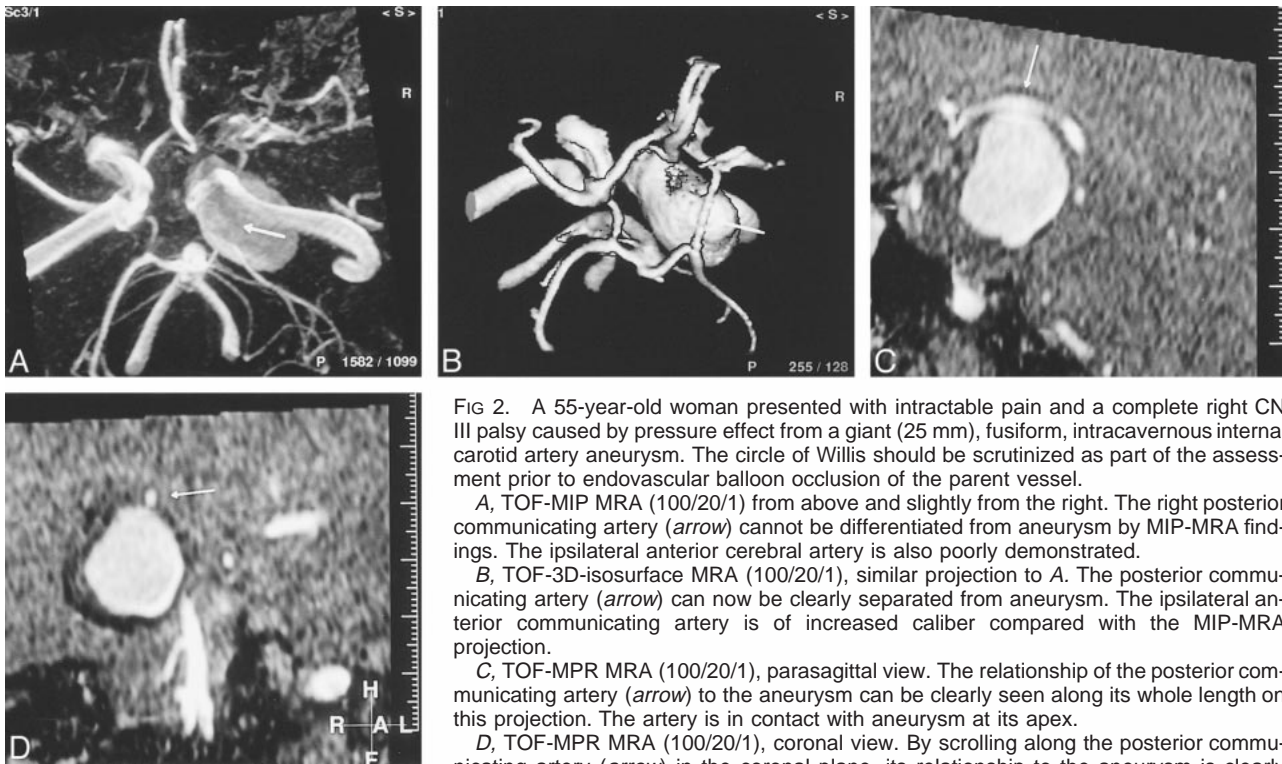In a 41-year-old man admitted for a SAH caused by rupture of a right posterior communicating ar-

FIG 2.   A 55-year-old woman presented with intractable pain and a complete right CN III palsy caused by pressure effect from a giant (25 mm), fusiform, intracavernous internal carotid artery aneurysm. The circle of Willis should be scrutinized as part of the assessment prior to endovascular balloon occlusion of the parent vessel.

A, TOF-MIP MRA (100/20/1) from above and slightly from the right. The right posterior communicating artery (*arrow*) cannot be differentiated from aneurysm by MIP-MRA findings. The ipsilateral anterior cerebral artery is also poorly demonstrated.

B, TOF-3D-isosurface MRA (100/20/1), similar projection to *A.* The posterior communicating artery (*arrow*) can now be clearly separated from aneurysm. The ipsilateral anterior communicating artery is of increased caliber compared with the MIP-MRA projection.

C, TOF-MPR MRA (100/20/1), parasagittal view. The relationship of the posterior communicating artery (*arrow*) to the aneurysm can be clearly seen along its whole length on this projection. The artery is in contact with aneurysm at its apex.

D, TOF-MPR MRA (100/20/1), coronal view. By scrolling along the posterior communicating artery (*arrow*) in the coronal plane, its relationship to the aneurysm is clearly depicted.
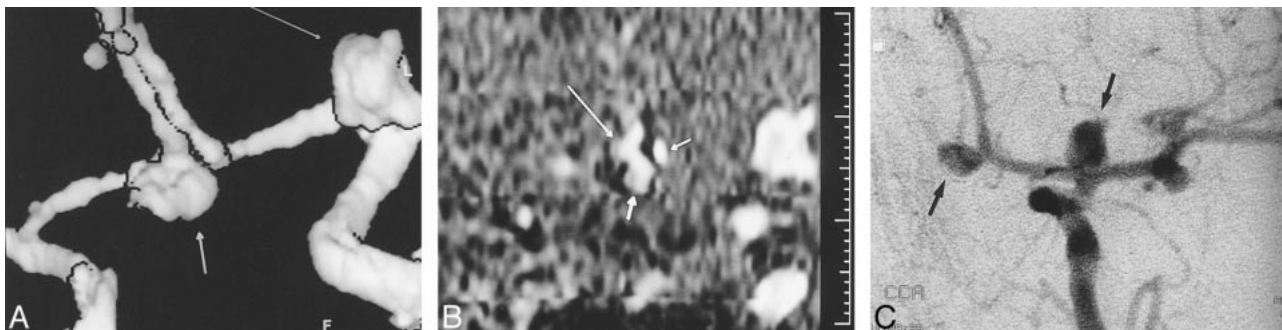

FIG 3.   A 48-year-old woman presented with an SAH secondary to an anterior communicating artery aneurysm rupture. Diagnostic IA-DSA showed multiple aneurysms.

A, TOF-3D-isosurface MRA (100/20/1), right periorbital view. There is some minor artifact due to patient movement. The anterior communicating artery aneurysm (*short broad arrow*) appears to arise from the right A1/A2 junction. A terminal left internal carotid artery aneurysm is also visible (*long thin arrow*).

B, TOF-MPR MRA (100/20/1), coronal slice through the anterior communicating artery complex. Scrolling through, no communication is seen between the left A1 segment (*thin short arrow*) and aneurysm (*short broad arrow*). The aneurysm is continuous with the right A2 segment (*long arrow*).

C, IA-DSA, left periorbital projection. The anterior communicating and left terminal internal carotid artery aneurysms are clearly seen (*arrows*). There are also two discrete middle cerebral artery aneurysms. The anterior communicating artery aneurysm only filled from a left-sided injection. If one were to have planned endovascular treatment on the basis of the MRA findings, the approach would have been via the right internal carotid artery.

tery aneurysm, a further right paraophthalmic-segment aneurysm was noted on the IA-DSA study. MRA, particularly when using MPR, suggested a 2-mm aneurysm involving the left middle cerebral artery bifurcation. This was confirmed by retrospective review of the original diagnostic angiogram. This area had originally been thought to represent overlying loops of vessels.

Case 3

MPR suggested an aneurysm between the right A1 and A2 segments of the anterior cerebral artery in a 48-year-old woman presenting with a ruptured anterior communicating artery aneurysm (Fig 3). The anterior communicating artery itself could not be seen. The axial source data suggested a narrow neck rising from the right side of the anterior com-

municating artery. The logical endovascular approach would have been via the right internal carotid artery if MRA had been used for preoperative planning. However, on an IA-DSA image, the aneurysm only filled from a left-sided injection. No filling was shown from the right side.

Case 4

IA-DSA poorly depicted the aneurysm in a 29-year-old man presenting with SAH secondary to a saccular anterior communicating artery aneurysm, which was obscured by an overlying A2 segment loop. This was well depicted on the 3D-isosurface images, partly because of the ability of this technique to allow viewing from any arbitrary direction.

Discussion

Many authors have demonstrated the diagnostic accuracy of MRA for the prospective detection of intracranial aneurysms (8, 12, 16, 17). Atlas et al (18) suggest that, although there has been significant technical improvement in MRA data acquisition, there has been little concomitant attention paid to image analysis. Most investigators have relied on the MIP algorithm, despite its recognized limitations. To this end, we attempted to estimate the clinical value of two post processing methods, MIP- and 3D-isosurface MRA, comparing them with a composite picture obtained from all imaging data, including those of IA-DSA images, in ruptured and unruptured intracerebral aneurysms. The method used to compare these techniques in the current study deserves consideration. The assessment of how well an imaging or visualization technique depicts regions of complex anatomy is predicated on the existence of a reference standard to which comparison can be made. In any study comparing a range of imaging and visualization techniques, it is clear that no such reference standard is available, because all of the techniques in the study are potentially subject to failure in some circumstances. In light of this, we have decided not to perform a simple comparison to IA-DSA because this could not, by definition, demonstrate any shortcomings in the depiction of morphology by IA-DSA itself. In an attempt to compensate for this, we have used a composite reference standard derived by review of all the imaging techniques available to describe the various features of the aneurysm and associated vascular anatomy. This technique is also subject to limitations. In particular, the use of a reference standard, which is a composite from multiple data sources, is difficult to present to the radiologists scoring the performance of the individual visualization methods. In view of this, we chose to have the same two scorers derive the composite reference standard and perform the subsequent scoring. Although this introduces the possibility of scoring bias, we believe that this type of comparison is valid in these circumstances.

Because the conversion of raw data into a processed image inevitably results in loss of or degradation of information (19), we included the source data in the form of axial images, as well as MPR images, into the study. It became clear during the study that, although source data images perform poorly compared with other visualizations, review of source data images prior to postprocessing is mandatory because of the problem of data reduction.

Velthuis et al (13) evaluated the diagnostic value of source images in combination with postprocessing techniques in 13 aneurysms by use of CT angiography (CTA). Source images viewed in cine mode were particularly useful for visualizing vessels close to bone (eg, ophthalmic and posterior communicating arteries) that were often poorly depicted by postprocessing techniques. The area close to the skull base and around the sphenoid sinus is also problematic for MRA, both because of susceptibility artifact due to adjacent bone and because of complex flow in the carotid siphon, causing signal loss as a result of phase incoherence. In these locations, MPR or axial source data images can be used to focus on an aspect of a known aneurysm such as the neck-to-fundus ratio, particularly if its orientation is known, without incurring loss or distortion of data due to postprocessing. MPR images have nearly the same spatial resolution as do the original axial images (20). With a working knowledge of an individual aneurysm's anatomic characteristics, important pretherapeutic information can be gained by selecting particular orthogonal or curved planes to highlight an area of interest; for example, an aneurysm's neck or a parent vessel. Scrolling through in selected planes allows one to extrapolate a sense of depth and create an internal image of a 3D structure. MPR was particularly useful in defining the neck, and also parent and branch vessels related to aneurysms in difficult locations.

Reference to the source images is also essential for establishing the presence of intramural hematoma (Fig 4). An established intraaneurysmal thrombus in large or giant aneurysms can readily be distinguished from intraluminal blood flow by its characteristic heterogeneous whorled pattern on axial source images (21). Subacute high T1 signal methemoglobin may be confused with flowing blood on TOF-MRA images, but this was not a problem we encountered in our study.

An analysis of the neck-to-fundus ratio is a crucial component of the preoperative evaluation of an aneurysm if one is considering endovascular intervention (3). Complex secondary flow patterns can result in signal loss through spin saturation and phase dispersion (6) and cause an apparent reduction in neck diameter. The relatively long echo time (7 ms) used in our TOF sequence can exacerbate signal loss, but this is compensated for partly by the small voxel size used to reduce intravoxel de-

FIG 4. A 62-year-old woman presenting with a left CN III palsy due to posterior communicating artery aneurysm.

A, IA-DSA of left common carotid artery, lateral projection. A large left, saccular, posterior communicating artery aneurysm with a discrete narrow neck is seen well.

B, TOF-MIP MRA (100/20/1), similar projection to that of *A.* Streamlining artifact is seen within the internal carotid artery, and there is signal loss within the aneurysm itself.

C, TOF-3D-isosurface MRA (100/20/1), similar projection to that of *A* and *B.* The posterior communicating artery aneurysm (*arrow*) appears identical to its depiction by IA-DSA.

D, Axial-source TOF image (100/20/1). The true lumen of the posterior communicating artery aneurysm is depicted as high signal, but this is surrounded by concentric mixed signal rims representing intramural thrombus (*arrow*). The presence of thrombus is not appreciated on the IA-DSA image. The aneurysm is significantly larger than the IA-DSA and postprocessed MRA images suggest.
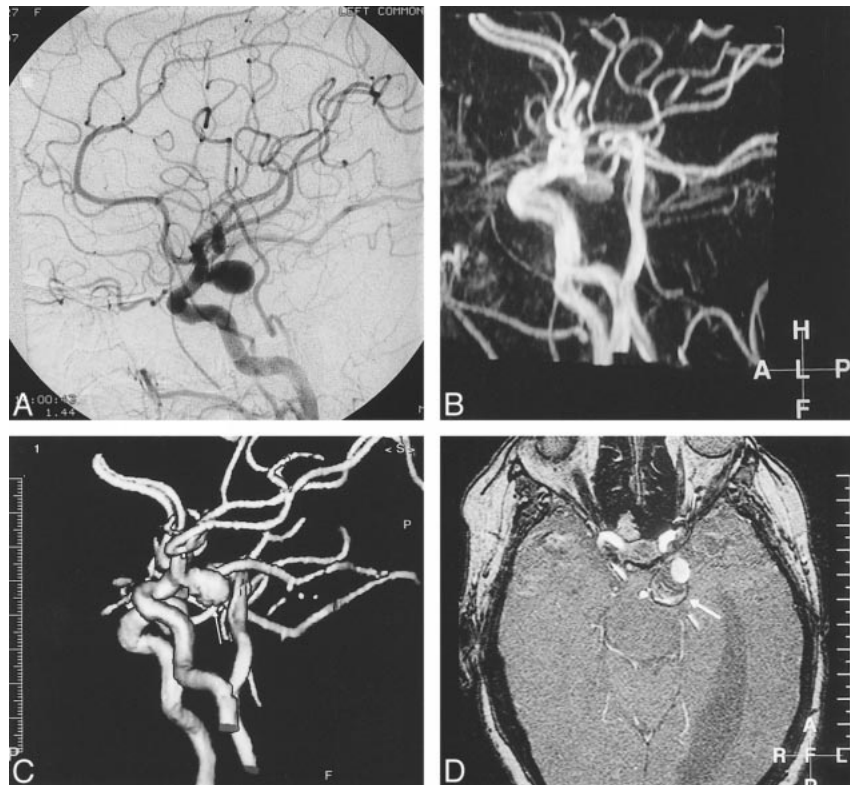
phasing. The application of shorter echo times will reduce the degree of signal void (22). Review of the source data and multiplanar images is also crucial in reducing inaccuracy of interpretation around the neck. Several observers have commented on the discrepancy between MR-reconstructed images and source data in assessing the degree of stenosis at the carotid bifurcation (23, 24, 25). Korogi et al (26) found that interpretation of source images rather than MIP images alone reduced reviewers' tendency to overestimate stenosis on MR angiograms in extracranial carotid disease. Close reference to source data in our study to produce the appropriate threshold level allowed a close correlation with the reconstructed 3D-isosurface MRA fingings, also reducing the potential for data loss.

Low-signal-intensity regions of a vessel may appear as "streamlining," or worse, may disappear completely on a MIP image (26). To be effective, visualization techniques should enhance the meaning and understanding of the data without corruption of these data. Because the MIP gray scale is derived from the composite value of all the pixels along an imaging plane, smaller structures may be assigned an inappropriately low signal intensity. This is an important limitation when dealing with aneurysms that may be as small as 2 mm. Small fluctuations in aneurysm morphology may also be underportrayed. The signal intensity of flow must exceed the maximum signal from the background noise, or it cannot be recognized as flow (27). Therefore, very slow flow close to the level of background noise may go undetected. In the presence of parabolic laminar flow, the reduced flow velocity, which occurs along a vessel wall, can result in false narrowing on MIP-MRA images. An alteration in the apparent morphology of an aneurysm, the misinterpretation of vessel spasm, or an exaggeration of vessel stenosis (28) are the direct results. It can also cause an erroneous impression of neck-to-fundus ratio, an important consideration when considering endovascular treatment (29), or fail to depict small vessels arising directly from an aneurysm itself. In one small saccular superior hypophyseal aneurysm directed medially, a signal void was created at the neck, leaving the aneurysm in midspace, apparently separated from its parent vessel. Appropriate thresholding with reference to the source data allowed the neck to be defined on 3D-isosurface MRA images.

A single MIP image also lacks depth. Because of confusing vessel overlap, a sense of disorientation on the part of the operator is produced, particularly around the complex middle cerebral artery bifurcation or trifurcation. The shaded surface algorithm of the isosurface MRA image makes this less problematic. Direct operator interaction, ie, rotation and manipulation of a 3D angiographic image in real time, is enhanced by an appropriate sense of depth, producing the higher scores of the isosurface MRA findings for depicting aneurysm morphology. The isosurface-rendered image is also far quicker in terms of interaction than an MIP reconstruction can be. For the isosurface-rendered images, a contour isosurface is extracted, which is relatively small in size. The majority of calcula-

tions required to rotate an isosurface have already been done during the initial rendering. Once a surface has been constructed, this can be rotated in the 3D viewing space within a matter of seconds. The problem with manipulating MIP images is that they are volume-rendered or ''splats.'' This means that for every rotational translation of the MIP, the projection rays for the entire image volume have to be recalculated. This involves manipulation of the entire volume data set, which is clearly sizeable. The extra time required to produce a particular projection increases the potential for a sense of disorientation on the part of the operator. In order to avoid this problem, it is common practice to process MIP reconstructions off-line, producing multiple renderings that can subsequently be viewed in a cine loop. It is, however, important to realize that these cine loops are not constructed from raw data at the time of viewing. The implications of this are that if a nonstandard projection is required, construction of new MIP projections will be slow to perform and, in addition, MIP reconstructions can not offer true ''real-time'' interactivity. This problem can be partially addressed by severe reduction of the data block by cropping, and real-time reconstruction can be obtained by use of graphics-optimized hardware. However, these hardware facilities are not provided on currently available commercial workstations and carry significant cost implications. Therefore, when deciding on the optimal angiographic projection for endovascular intervention, we chose the 3D-isosurface technique over MIP reconstructions.

A single-slab TOF technique was used in the present study. Theoretically this is susceptible to edge-of-field saturation effects, but because of the central location of most of the aneurysms in the study, around the circle of Willis, this did not prove to be a problem. It should be stressed, however, that the imaging protocol used in this study reflects the capabilities of the imaging system at the beginning of the study. The use of shorter echo times than those employed herein will reduce intravoxel phase loss in areas of nonlaminar flow, such as in aneurysm necks. If this is combined with the use of a variable flip angle technique, such as tilted optimized nonsaturation excitation to compensate for progressive saturation of spins travelling through the volume, then signal characteristics will also be more consistent.

Three-dimensional–isosurface MRA was significantly superior to MIP-MRA for aneurysm detection, depiction of aneurysm morphology, and confidence in neck and branch vessel interpretation. The isosurface algorithm creates a 3D surface based on the identification of an image intensity contour selected using an operator set threshold. Once the surface is computed, rotation can be performed in real time on most platforms, because the algorithms employed are not computationally intensive. Because of its subjective nature, the technique demands some technical expertise. A learning curve was encountered in the selection of the appropriate threshold level prior to the commencement of the study. With experience, we appreciated that variability can be minimized if the threshold chosen concurs with the source data, ie, the source data should first be analyzed and then a threshold set that includes all the information seen on the source image. Inappropriate thresholding may result in the inclusion of background noise in the processed image (29). This can produce an overestimate of neck size, and suggest that an aneurysm is unfavorable for endovascular treatment. Conversely, setting the threshold too high may have the opposite effect. In the presence of perianeurysmal hematoma, the ability to set a defined threshold may have advantages. Judicious targeting with reference to the source images can remove much of the artifact created by high T1 signal methemoglobin. This is not possible with the MIP algorithm, which is not threshold-dependent. Perianeurysmal hematoma is therefore another explanation for poor scoring rendered using the MIP technique. Conversion of oxyhemoglobin to methemoglobin within the subarachnoid space can be delayed because of the higher oxygen tension within CSF when compared with brain (30). Theoretically, prompt MR examination before the formation of breakdown products while blood within CSF is still hypointense may lessen this effect, but this was not noticeable in our small series. The presence of significant parenchymal hematoma makes reconstruction using either technique more prone to error.

Wilcoxon ranking showed that 3D-isosurface MRA findings were comparable to those of IA-DSA in aneurysm morphology on Wilcoxon ranking (Table 2), and on overall average scores only slightly underscored IA-DSA (Fig 1). The ability to manipulate an image in real time, the spatial awareness produced by the shaded surface rendering and selective targeting to remove overlying vessels contributed to this. For example, in one anterior communicating artery aneurysm (Fig 5), fenestration of the anterior communicating artery was not appreciated on limited-projection diagnostic IA-DSA images, but was apparent on isosurface renderings. The ability to view images in multiple planes is a clear advantage of MRA over a limited IA-DSA study. Three-dimensional–isosurface MRA could also be used to confirm the fusiform nature of giant cavernous internal carotid artery aneurysms. Sometimes the nature of such an aneurysm can only be assumed on the basis of conventional angiography findings, despite multiple projections.

Relatively few investigators have directly correlated MRA and CT angiography (CTA) (31–33). CTA has the advantage that it can readily be performed immediately after the unenhanced CT has confirmed an SAH. There is no contraindication to scanning those patients who would be unsuitable for MRA, such as critically ill patients, patients with claustrophobia, and those with pacemakers, al-
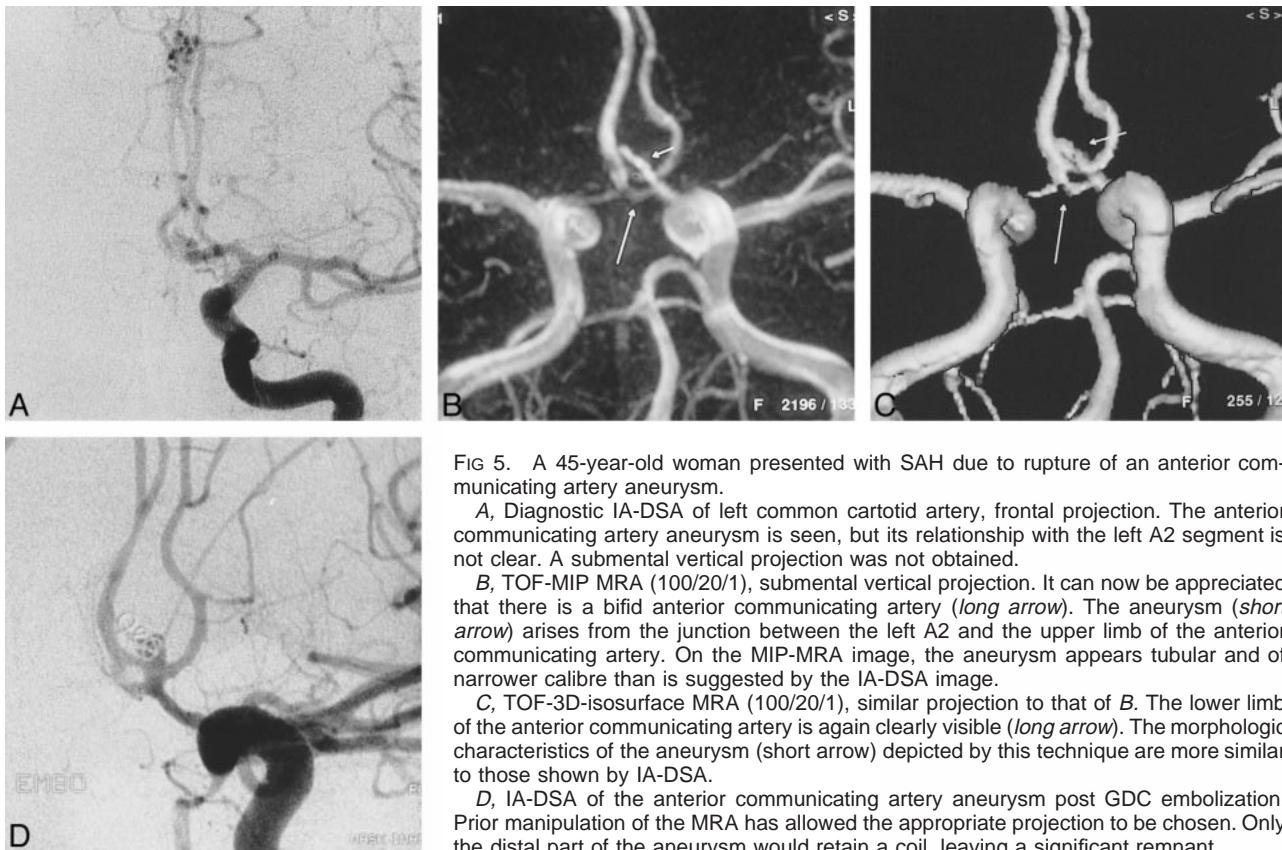
Fig 5. A 45-year-old woman presented with SAH due to rupture of an anterior communicating artery aneurysm.

A, Diagnostic IA-DSA of left common cartotid artery, frontal projection. The anterior communicating artery aneurysm is seen, but its relationship with the left A2 segment is not clear. A submental vertical projection was not obtained.

B, TOF-MIP MRA (100/20/1), submental vertical projection. It can now be appreciated that there is a bifid anterior communicating artery (*long arrow*). The aneurysm (*short arrow*) arises from the junction between the left A2 and the upper limb of the anterior communicating artery. On the MIP-MRA image, the aneurysm appears tubular and of narrower calibre than is suggested by the IA-DSA image.

C, TOF-3D-isosurface MRA (100/20/1), similar projection to that of *B.* The lower limb of the anterior communicating artery is again clearly visible (*long arrow*). The morphologic characteristics of the aneurysm (short arrow) depicted by this technique are more similar to those shown by IA-DSA.

D, IA-DSA of the anterior communicating artery aneurysm post GDC embolization. Prior manipulation of the MRA has allowed the appropriate projection to be chosen. Only the distal part of the aneurysm would retain a coil, leaving a significant remnant.

though CTA may be inadequate in those patients with left ventricular failure due to suboptimal opacification of the intracranial vasculature (34). One of the limitations of CTA, particularly when using shaded surface display or 3D-isosurface reconstruction, is the inherent difficulty of detecting small aneurysms in close proximity to the skull base or cavernous sinus. Because a threshold density of approximately 100 HU must be set to exclude brain, hemorrhage, and fat (34), high-density structures such as opacified veins, infundibulum, choroid plexus, and bone can be incorporated into the reconstructed image. Bone can be edited out of the reconstructed image, but this requires time, patience, and is open to error despite a thorough knowledge of anatomy. Ogawa et al (35) examined 73 aneurysms measuring from 2 to 32 mm in 65 patients by use of CTA, looking only at surface-rendered images, without reference to axial source data. They recommended its use in the preoperative evaluation of large and giant aneurysms, but found it less useful in aneurysms with diameters of 5 mm or less. Hope et al (36) also advocated caution regarding the use of screening CTA for the detection of smaller aneurysms. As with TOF-MRA, problems may be encountered with separating a high-attenuation blood clot from intravascular contrast medium on CTA images (36).

Huston et al (37) found advantages of the phase-contrast (PC)-MRA technique over TOF-MRA, because of its variable sensitivity to velocity, low sensitivity to saturation effects, and superior background suppression. However, flow direction within an aneurysm can oscillate during the cardiac cycle (38). Pulsatile flow, because of the necessity for subtraction, can result in artifacts. This contributes to the signal loss of the PC-MRA technique. Flow velocity within an aneurysm can be much slower than in the parent vessel. Setting the appropriate velocity encoding profile to accommodate both aneurysm and vessel is impractical. Black-blood MRA, which highlights the vessel lumen by making flowing blood appear black in contrast to the surrounding static tissue (6), should have advantages over TOF- and PC-MRA, particularly in regions of complex flow. In fact, spin dephasing, which is problematic in bright-blood techniques, contributes to the desired signal loss (39). However, black-blood MRA is limited by the signal void that occurs around the skull base and its inability to differentiate thrombus from true lumen (20). A potential solution to the problem of slow flow and spin dephasing in the TOF technique is the use of contrast agents to shorten the T1 of flowing blood (40, 41). The use of ultrashort repetition times to reduce total acquisition to less than 1 minute can further overcome saturation effects (42).

Although it provides important information about anatomic location and morphology, TOF-MRA per se does not provide hemodynamic information, although newer techniques may rectify this (43). This was highlighted by the anterior com-

municating artery aneurysm (Fig 3) that appeared to lie between the right A1 and A2 segments of the anterior cerebral artery, but filled from a left-sided injection during conventional angiography. The patient was successfully coiled by way of a left-sided approach. Sometimes during an endovascular procedure, for mechanical reasons or because of thromboembolic complications, a vessel may be lost (eg, an A2 segment of the anterior cerebral artery). One needs to know a priori the supply of the two distal A2 segments; ie, whether they have unilateral or dual supply via the anterior communicating artery from the A1 segments. Similarly, the adequacy of a posterior communicating artery in endosaccular embolization of a basilar termination aneurysm cannot be inferred from an MRA examination. One possible approach to this is the use of oblique presaturation slabs overlying one carotid artery during TOF acquisition. However, although this allows assessment of the contribution from each carotid in the resting state, it does not depict the flow changes that will result if vessel occlusion occurs. The use of IA-DSA combined with carotid compression remains the only available method for attempting to predict the results of this type of hemodynamic insult.

In conclusion, TOF-MRA can be a useful adjunct to conventional angiography in the assessment of intracerebral aneurysms. It is particularly useful in difficult anatomic situations, such as the middle cerebral artery bifurcation or anterior communicating artery complex. It is also useful in the delineation of intraaneurysmal thrombus. If MRA is used in aneurysm assessment, meticulous technique and reference to the source data are mandatory. Three-dimensional–isosurface reconstruction is consistently more reliable than are MIP reconstructions.

References

1. Guglielmi G, Vinuela F, Sepetka I, Macellari V. **Electrothrombosis of saccular aneurysms via endovascular approach. Part 1. Electrochemical basis, technique and experimental results.** *J Neurosurg* 1991;75:1–7
2. Guglielmi G, Vinuela F, Dion J, Duckwiler G. **Electrothrombosis of saccular aneurysms via endovascular approach. Part II: Preliminary clinical experience.** *J Neurosurg* 1991;75:8–14
3. Fernandez Zubillaga A, Guglielmi G, Vinuela F, Duckwiler G. **Endovascular occlusion of intracranial aneurysms with electrolytically detachable coils: correlation of aneurysm neck size and treatment results.** *AJNR Am J Neuroradiol* 1994;15:815–820
4. Byrne JV, Guglielmi G. **Treatment by endosaccular packing with the Guglielmi detachable coil.** In: Byrne JV, Guglielmi G, eds. *Endovascular Treatment of Intracranial Aneurysms.* Berlin: Springer Verlag;1998;1:134–163
5. Heiserman JE, Dean BL, Hodak JA et al. **Neurological complications of cerebral angiography.** *AJNR Am J Neuroradiol* 1994;15:1401–1407
6. Graves MJ. **Magnetic resonance angiography. Review article.** *Br J Radiol* 1997;70:6–28
7. Huston J III, Nichols DA, Luetmer PH, et al. **Blinded prospective evaluation of sensitivity to MR angiography to known intracranial aneurysms: importance of aneurysm size.** *AJNR Am J Neuroradiol* 1994;15:1607–1614
8. Litt AW. Commentary. **MR angiography of intracranial aneurysms: proceed, but with caution.** *AJNR Am J Neuroradiol* 1994;15:1615–1616
9. Sankhla SK, Gunawardena WJ, Coutinho CMA, Jones AP, Keogh AJ. **Magnetic resonance angiography in the management of aneurysmal subarachnoid hemorrhage: a study of 51 cases.** *Neuroradiology* 1996;38:724–729
10. Anderson CM, Saloner D, Tsuruda JS, Shapeero LG, Lee RE. **Artifacts in maximum-intensity-projection display of MR angiograms.** *AJNR Am J Neuroradiol* 1990;154:623–629
11. Bosmans H, Wilms G, Marchal G, Demaerel P, Baert AL. **Characterization of intracranial aneurysms with MR angiography.** *Neuroradiology* 1995;37:262–266
12. Nakajima S, Atsumi H, Bhalero AH, et al. **Computer-assisted surgical planning for cerebrovascular surgery.** *Neurosurgery* 1997;41:403–408
13. Velthuis BK, van Leeuwen MS, Witkamp TD, et al. **CT angiography: source images and postprocessing techniques in the detection of cerebral aneurysms.** *AJR Am J Roentgenol* 1997;169:1411–1417
14. Velthuis BK, Rinkel GJ, Ramos LM, et al. **Subarachnoid hemorrhage: aneurysm detection and preoperative evaluation with CT angiography.** *Radiology* 1998;208:423–430
15. Altman DG. *Practical Statistics for Medical Research.* Edinburgh: Chapman Hall;1991
16. Grandin CB, Mathurin P, Stroobandt G, Hammer F, Goffette, Cosnard G. **Diagnosis of intracranial aneurysms: accuracy of MR angiography at 0.5 T.** *AJNR Am J Neuroradiol* 1998;19:245–252
17. Curnes JT, Shogry MEC, Clark DC, Elsner HJ. **MR angiographic demonstration of an intracranial aneurysm not seen on conventional angiography.** *AJNR Am J Neuroradiol* 1993;14:971–973
18. Atlas SW, Sheppard L, Goldberg HJ, Hurst RW, Listerud J, Flamm E. **Intracranial aneurysms: detection and characterization with MR angiography with use of an advanced postprocessing technique in a blinded-reader study.** *Radiology* 1997;203:807–814
19. Schreiner S, Paschal CB, Galloway RL. **Comparison of projection algorithms used for the construction of maximum intensity projection images.** *J Comput Assist Tomogr* 1996;20:56–67
20. Rubinstein D, Sandberg EJ, Breeze RE, et al. **T2-weighted three-dimensional turbo spin-echo MR of intracranial aneurysms.** *AJNR Am J Neuroradiol* 1997;18:1939–1943
21. Brugieres P, Blustajn J, Le Guerinel C, Meder JF, Thomas P, Gaston A. **Magnetic resonance angiography of giant intracranial aneurysms.** *Neuroradiology* 1998;40:96–102
22. Lin W, Tkach JA, Haacke EM, Masaryk TJ. **Intracranial MR angiography: application of magnetization transfer contrast and fat saturation to short gradient-echo, velocity-compensated sequences.** *Radiology* 1993;186:753–761
23. Huston J III, Lewis BD, Wiebes DO, Meyer FB, Riederer SJ, Weaver AL. **Carotid artery: prospective blinded comparison of two-dimensional time-of-flight MR angiography with conventional angiography and duplex US.** *Radiology* 1993;186:339–344
24. Anderson CM, Lee RE, Levin DL, et al. **Measurement of internal carotid artery stenosis from source MR angiograms.** *Radiology* 1994;193:219–226
25. De Marco JK, Nesbit GM, Wesbey GE, Richardson D. **Prospective evaluation of extracranial carotid stenosis: MR angiography with maximum-intensity projections and multiplanar reformation compared with conventional angiography.** *AJR Am J Roentgenol* 1994;163:1205–1212
26. Korogi Y, Takahashi M, Nakagawa T, et al. **Intracranial vascular stenosis and occlusion: MR angiographic findings.** *AJNR Am J Neuroradiol* 1997;18:135–143
27. Atlas SW, Listerud J, Chung W, Flamm ES. **Intracranial aneurysms: depiction on MR angiograms with a multifeature-extraction, ray-tracing postprocessing algorithm.** *Radiology* 1994;192:129–139
28. Wentz KU, Rother J, Scwartz A, Mattle HP, Suchalla R, Edelman RR. **Intracranial vertebrobasilar system: MR angiography.** *Radiology* 1994;190:105–110
29. Bontozoglou NP, Spanos H, Lasjaunias P, Zarifis G. **Intracranial aneurysms: endovascular evaluation with three-dimensional-display MR angiography.** *Radiology* 1995;197:876–879
30. Ida M, Kurisu Y, Yamashita M. **MR Angiography of ruptured aneurysms in acute subarachnoid hemorrhage.** *AJNR Am J Neuroradiol* 1997;18:1025–1032
31. Schwartz RB, Tice HM, Hooten SM, Hsu L, Stieg PE. **Evaluation of cerebral aneurysms with helical CT: correlation with conventional angiography and MR angiography.** *Radiology* 1994;192:717–722
32. Holtas S, Olsson M, Romner B, Larsson EM, Saveland H, Brandt L. **Comparison of MR imaging and CT in patients with intracranial aneurysm clips.** *AJNR Am J Neuroradiol* 1988;9:891–897

33. Harrison MJ, Johnson BA, Gardner GM, Welling BG. **Preliminary results on the management of unruptured intracranial aneurysms with magnetic resonance angiography and computed tomographic angiography.** *Neurosurgery* 1997;40:947–955
34. Vieco PT. **CT angiography of the intracranial circulation.** *Neuroimaging Clin North Am* 1998;8:577–592
35. Ogawa T, Okudera T, Noguchi K, et al. **Cerebral aneurysms: evaluation with three-dimensional CT angiography.** *AJNR Am J Neuroradiol* 1996;17:447–454
36. Hope JKA, Wilson JL, Thomson FJ. **Three-dimensional CT angiography in the detection and characterization of intracranial berry aneurysms.** *AJNR Am J Neuroradiol* 1996;17:439–445
37. Huston J III, Rufenacht DA, Ehman RL, Wieben DO. **Intracranial aneurysms and vascular malformations: comparison of time-of-flight and phase contrast MR angiography.** *Radiology* 1991;181:721–730
38. Araki Y, Kohmura E, Tsukaguchi I. **A pitfall in detection of intracranial unruptured aneurysms on three-dimensional phase-contrast MR angiography.** *AJNR Am J Neuroradiol* 1994;16:1618–1623
39. Edelman RR, Mattle HP, Wallner B, et al. **Extracranial carotid arteries: evaluation with "black blood" MR angiography.** *Radiology* 1990;177:45–50
40. Bosmans H, Marchal G. **Contrast-enhanced MR angiography.** *Radiology* 1996;36:115–123
41. Kouwenhoven M. **Contrast-enhanced MR angiography. Methods, limitations and possibilities.** *Acta Radiol Suppl* 1997;412:57–67
42. Talagala SL, Jungreis CA, Kanal E, et al. **Fast three-dimensional time-of-flight MR angiography of the intra-cranial vasculature.** *Magn Reson Imaging* 1995;5:317–323
43. van Everdingen KJ, Visser GH, Klijn CJ, Kappelle LJ, van der Grond J. **Role of collateral flow on cerebral hemodynamics in patients with unilateral internal carotid artery occlusion.** *Ann Neurol* 1998;44:167–176